

Acoustic vibrations in free-standing double layer membranes

R. S. Bandhu, X. Zhang, and R. Sooryakumar

Department of Physics, The Ohio State University, Columbus, Ohio 43210, USA

K. Bussmann

Naval Research Laboratory, Washington, DC 20375, USA

(Received 5 March 2004; revised manuscript received 3 May 2004; published 23 August 2004)

We report on a Brillouin light scattering study of acoustic excitations in free-standing polymethyl methacrylate (PMMA)/Si₃N₄ double layer membranes. For vanishing-wave vector transfer along the membrane, the observed excitations are a series of longitudinal standing wave harmonics whose frequencies depend on PMMA and Si₃N₄ layer thickness. The associated displacement profiles below 30 GHz are largely confined to the softer PMMA layer with mode amplitudes significantly higher at the PMMA surface than at the free surface of the high elastic modulus Si₃N₄ layer. At higher frequencies, in the vicinity and beyond the resonance associated with the Si₃N₄ layer, the mode amplitudes become comparable at both free surfaces. Excitations with transverse polarization as well as waves whose amplitudes within the Si₃N₄ are consistent with flexural and dilatational modes for a single layer are also observed. For certain ranges of wave vector the latter interact and hybridize with the harmonics arising from the PMMA layer.

DOI: 10.1103/PhysRevB.70.075409

PACS number(s): 68.60.Bs, 63.22.+m, 62.25.+g, 78.35.+c

The mechanical and electrical properties of micro- and nano-electromechanical systems (MEMS/NEMS)¹⁻⁴ are of current interest not only for their underlying technological value that range from ultrasensitive sensors to drug delivery systems but also for the opportunities they provide for fundamental science. Recently, increased interest in freestanding double layer membranes,⁵ especially where one of the layers is a polymer, has begun to emerge. This activity stems from the fact that synthetic polymers offer a wealth of opportunities to design responsive structures that are triggered by external local stimuli such as light and heat. While the reduced dimensions and mass give these freestanding single- and double layer membranes unique technological advantages, it is these same compact features that challenge characterization of their mechanical/elastic properties. Such properties, in turn, underlie many of the applications as well as fundamental physics offered by these mesoscopic mechanical structures. The latter include vibrations in flexural nanoresonators⁶, quantized phonon transport,⁷ and search for the quantum limit to thermal conductance.⁸ In addition to the acoustic resonances in suspended membranes, associated flexural oscillations are predicted to influence the low temperature thermal conductance and the relaxation rate of electrons.^{9,10} Since the flexural and dilatational modes of a double layer structure can be strongly altered from those allied with a single layer, important differences in the thermal properties of a membrane can be expected when it is configured within freestanding double layer structures. These differences are expected to be especially relevant in dielectric and semiconductor structures where heat flow is most often dominated by phonon transfer.

In this paper we report on a Brillouin light scattering study on the elastic properties of freestanding poly(methyl methacrylate)/silicon nitride [PMMA/Si₃N₄] double layer nanomembranes. While the polymer is soft and widely used as positive resist for high-resolution electron beam, deep ultraviolet (220–250 nm) and x-ray lithographic processes, by

contrast, the Si₃N₄ layer is a hard, high elastic modulus material. This large elastic mismatch strongly influences the acoustic properties of the freestanding structure leading to confinement of discrete, longitudinal, and transverse polarized low frequency (≤ 30 GHz) acoustic standing waves primarily within the polymer layer. Their transformation to traveling higher order Lamb waves is revealed when the propagation wave vector is tuned away from the membrane normal. At higher frequencies, where the Si₃N₄ membrane supports discrete standing wave resonances,¹¹ the acoustic mode profiles permeate and extend throughout both double layer components. The experiments also reveal elastic waves whose amplitudes of vibration within the Si₃N₄ are consistent with flexural and dilatational traveling modes for a single layer of Si₃N₄ of the same thickness.¹¹ For a specific range of wave vectors these modes couple and hybridize with the harmonics arising from the softer PMMA layer.

The PMMA/Si₃N₄ double layer membranes were fabricated using commercially supplied low-pressure chemical vapor deposition silicon nitride coated (100) oriented silicon wafers. The Si₃N₄ layer thickness (d_s) in each instance was fixed at 100 nm. Standard potassium hydroxide (KOH) backside etching techniques were used to remove the Si substrate to produce a Si₃N₄ membrane window of 4×4 mm dimensions. PMMA (Microchem Corp., Newton, Massachusetts, 2%/950 K in anisol) was spin coated over the membrane at speeds ranging from 4–8 kilo-RPM and postbaked at 150°C for 45 min. The thicknesses were determined using a spectroscopic thin film analyzer and we report on measurements from three double layer samples with PMMA layer thickness (d_p) of 55, 75, and 115 nm. Given the relevant dimensions of the experiment [phonon wavelength (~ 300 nm), laser spot focus (~ 40 μ m)], these double layers can hence be treated as free standing. Brillouin light scattering (BLS) measurements were performed in back-scattering ($p \rightarrow p+s$) at ambient temperature using approximately 50 mW p -polarized

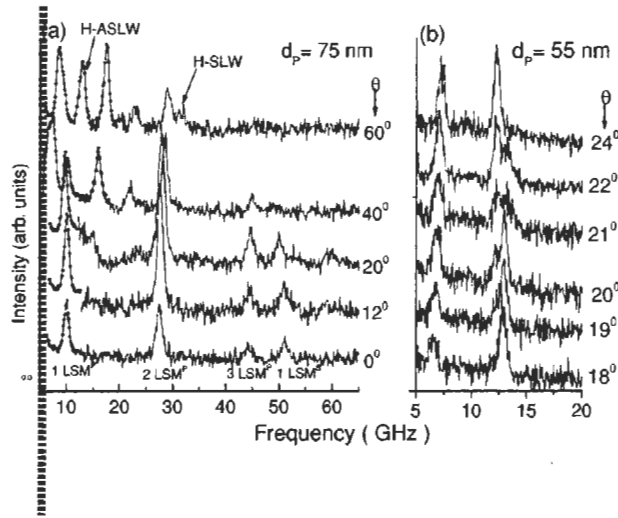


FIG. 1. (a) Typical Brillouin spectra recorded from a double layer structure consisting of 100 nm (d_S) Si_3N_4 and 75 nm (d_P) PMMA membranes. Peaks observed for an angle of incidence $\theta = 0^\circ$, are due to the lowest lying longitudinal standing waves 1–3 LSM^P and 1 LSM^S . With increasing θ , transverse, flexural, and dilatational type modes emerge. The low frequency data connected by a solid line have been reduced by a factor of three. (b) Spectra recorded from the $d_P=55$ nm structure over a narrow range of θ ($18^\circ \leq \theta \leq 24^\circ$) illustrating the hybridized H-SLW and 1 LSM^P modes around 12 GHz.

$\lambda=514.5$ nm radiation. At these power density levels, no evidence of photodegradation in the PMMA or Si_3N_4 layers was evident. The standing wave excitations were most clearly observed at small scattering angles θ , where θ is the deviation of the back-scattered beam from the double layer normal. Measurements were recorded when θ increased from $\sim 0^\circ$ to 70° thereby monitoring the dispersion and transformation of discrete K_\perp (wave vector component perpendicular to membrane) standing wave resonances to traveling modes with dominant in-plane wave vector $K_{||}[(=4\pi/\lambda)\sin\theta]$ character.

Figure 1(a) shows BLS spectra recorded from the 75 nm(d_P)/100 nm(d_S) [$\text{PMMA}/\text{Si}_3\text{N}_4$] double layer membranes for $0^\circ \leq \theta \leq 60^\circ$ i.e., its variation with $K_{||}$. The peaks at 10 and 27 GHz evident from the $\theta=0^\circ$ spectra are excitations with nominally vanishing $K_{||}$. These excitations are respectively identified as the $N=1$ and 2 order longitudinal standing modes (1 LSM^P , 2 LSM^P) whose amplitude variation within the PMMA layer is very close to that of a standing wave with an approximate node and an antinode at the interface and free surface, respectively. Evidence of the next modes in this sequence, 3 LSM^P and 4 LSM^P , is found at ~ 44 and ~ 60 GHz in the spectra [Fig. 1(a)] recorded at $\theta=20^\circ$. The excitation at 52 GHz, is the longitudinal standing mode (1 LSM^S) closely associated with the lowest standing wave resonance in a Si_3N_4 layer.¹¹ Additional modes observed at higher θ include (i) the $N=1, 2$ transverse standing wave (1 TSM^P , 2 TSM^P) allied primarily with the PMMA layer and, (ii) the hybridized symmetric and antisymmetric Lamb wave (H-SLW, H-ASLW) modes originating mainly

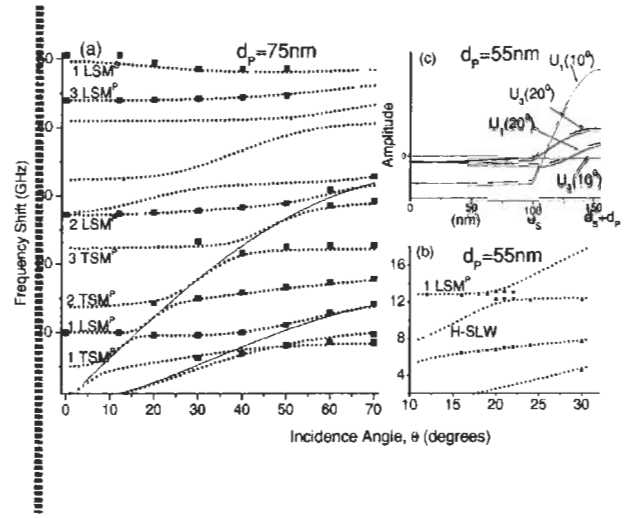


FIG. 2. (a) Dispersion of modes in the unsupported double layer structure with $d_S=100$ nm (Si_3N_4) and $d_P=75$ nm (PMMA). The experimental data are indicated by squares and the circular dots represent calculated mode frequencies. Thin solid lines are the SLW (higher frequency) and ASLW (lower frequency) modes associated with a 100 nm thick freestanding Si_3N_4 membrane. (b) Dispersion from the $d_P=55$ nm structure showing hybridization between H-SLW and 1 LSM^P for special angles θ . (c) The mode amplitudes $U_1(\theta)$ and $U_3(\theta)$ calculated for H-SLW at $\theta=10^\circ$ (thin line) and $\theta=20^\circ$ (dark line) as a function of the distance (in nanometer) from the free surface of the Si_3N_4 membrane.

from the Si_3N_4 layer¹¹. We note that away from $\theta \sim 0^\circ$ the classification of the modes as longitudinal and transverse, though approximate, provides a framework to readily understand the main physical character of the modes as inferred from the acoustic displacement fields calculated by the theoretical model presented below. Figure 1(b) shows spectra recorded from the $d_P=55$ nm structure over a narrow spread in θ ($18^\circ \leq \theta \leq 23^\circ$). These spectra, as discussed below, reveal the hybridization that occurs at ~ 12 GHz when the dilatational type traveling mode associated with a Si_3N_4 layer of thickness $d_S=100$ nm interacts with the low frequency harmonic 1 LSM^P .

We now turn to the projected local density of states (PLDOS) D_i that provide for the dispersion and mode amplitudes of the double layer vibrations. This is evaluated within a Green's function formalism

$$D_i(\omega^2, K, x_3 = z) = -(\pi)^{-1} \text{Im } G_{ii}(K, x_3 = z, \omega^2).$$

Here i refers to the mode polarization. G_{ii} is the (x_i, x_i) component of the Fourier (frequency and wave vector) domain elastodynamic Green's function tensor for depth x_3 from the membrane surface. The method of calculation of G_{ii} is provided in Ref. 12.

Figure 2(a) illustrates the mode dispersions for the $d_P=75$ nm double layer membrane as a function of scattering angle θ (and hence of $K_{||}$). The frequencies of the measured phonon peaks are identified by the square symbols. The best fits (circular dots) to the data shown in Fig. 2(a) as well as corresponding data from the other double layer struc-

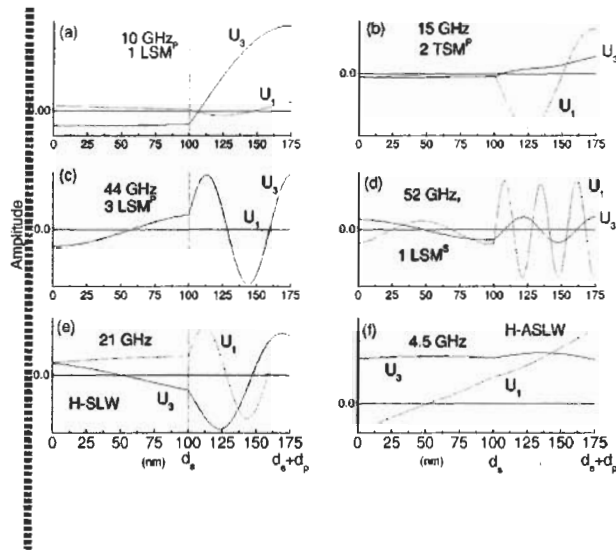


FIG. 3. Calculated mode displacements U_1 (dotted line) and U_3 (solid line) across the thickness of the freestanding double layer for the structure $d_S=100$ nm and $d_p=75$ nm corresponding to Figs. 1 and 2. (a), (c), and (d) are calculated for $\theta=12^\circ$ while (b) and (e) are determined at $\theta=40^\circ$ and (f) is evaluated at $\theta=30^\circ$.

tures (not shown) were obtained by using a single set of elastic constants for the Si_3N_4 and PMMA ($C_{11}^{\text{SiN}}=283.6$ GPa; $C_{44}^{\text{SiN}}=85.4$ GPa; $C_{11}^{\text{PMMA}}=8.8$ GPa; $C_{44}^{\text{PMMA}}=2.4$ GPa) and their known densities ($\rho^{\text{SiN}}=2.8$ g/cm³; $\rho^{\text{PMMA}}=1.18$ g/cm³).

The phonon dispersion reveals a series of discrete excitations which, at small scattering angles, are identified as the longitudinal and transverse standing wave resonances (≤ 30 GHz) displaying significant amplitude variation within the PMMA layer. Consistent with the very soft PMMA elastic modulus, the lower order ($N=1-2$) resonances associated with this layer are observed below 30 GHz, with neighboring orders separated by 17 GHz (for LSM^P) and 9.5 GHz (for TSM^P). Analysis of the mode displacement U_3 (normal to membrane plane) and U_1 (in sagittal plane, along K_{II}) of 1LSM^P ($\theta=12^\circ$) and 2TSM^P ($\theta=40^\circ$) is shown in Figs. 3(a) and 3(b). In addition to confirming their strong polarized features, the displacement profiles reveal their confinement mainly within the polymeric layer with limited variation in the hard Si_3N_4 membrane.

For $\theta \sim 0^\circ$ the mode amplitudes of the low frequency excitations such as 1LSM^P and 1TSM^P is akin to that in an organ-pipe with one end closed (PMMA/ Si_3N_4 interface) and the other open (free PMMA surface).¹³ The Si_3N_4 layer thus acts effectively as a barrier to these excitations within the PMMA layer. For frequencies far removed from the resonances associated with a single Si_3N_4 layer, the amplitudes at the PMMA/ Si_3N_4 interface approximate a node and an antinode at the free PMMA surface. The corresponding frequencies are hence approximated by $f_n = [(2n+1)V_{T,L}^P]/4d_p$ where V_T^P and V_L^P represent the transverse and longitudinal velocity of the PMMA layer. At $\theta=0^\circ$, i.e., with vanishing K_{II} and finite normal wave-vector (K_{\perp}) components, the LSM^P (TSM^P) modes are pure longitudinal (transverse) hav-

ing only U_3 (U_1) displacement. At 44 GHz, corresponding to the frequency of 3LSM^P , the amplitude at the interface is poorly represented by a nodal point. As evident from Fig. 3(c) at this higher frequency 3LSM^P approaches the lowest standing wave resonance 1LSM^S (52 GHz) characteristic of the hard Si_3N_4 layer leading, in turn, to greater penetration into the nitride layer. Moreover, at 52 GHz (1LSM^S) it is evident from Fig. 3(d), that while a complete half-wave is confined within the nitride layer, the amplitude permeates into the softer PMMA layer yielding a profile with significant amplitudes in both membrane components of the double layer. In this case their frequencies are well approximated by $f_n = nV_L^S/2d_S$ where V_L^S is the longitudinal velocity corresponding to the Si_3N_4 layer.

From the calculated dispersion [Fig. 2(a)] it is evident that, besides the discrete standing wave resonances discussed above, two additional modes are predicted. The dispersion of these two excitations, when uncoupled to other double layer excitations, is very similar to that of the symmetric- and antisymmetric-Lamb waves (SLW and ASLW) from a single Si_3N_4 membrane of thickness d_S .¹¹ The dispersion of corresponding modes from a single Si_3N_4 layer is indicated by the thin solid lines in Fig. 2(a). The higher frequency mode of this pair in the double layer, H-SLW, is strongly dispersive and hybridizes with low lying discrete harmonics associated with the PMMA membrane yielding characteristic mode repulsion and opening of a gap in the dispersion [Fig. 2(a)]. Other evidence of acoustic mode hybridization has been observed between the Rayleigh wave and the longitudinal resonance in bulk Si with a patterned periodic grating on the surface.¹⁴ The lower frequency mode (H-ASLW) reveals a relatively modest variation in frequency (~ 10 GHz) for $0^\circ \leq \theta \leq 70^\circ$. In this case its hybridization with 1TSM^P for $\theta \sim 30^\circ - 45^\circ$ is revealed by a frequency downshift compared to that in a single Si_3N_4 membrane in Fig. 2(a). Figures 3(e) and 3(f) illustrate the mode amplitudes associated with H-SLW and H-ASLW at 21 and 4.5 GHz calculated for $\theta \sim 40^\circ$ and 30° , respectively. The profiles of the H-SLW and H-ASLW modes inside Si_3N_4 of the double layer are similar to that of SLW and ASLW in a single Si_3N_4 membrane, respectively.¹¹

Experimental confirmation of the coupling between H-SLW and 1LSM^P is evident in Fig. 1(b) recorded for the $d_p=55$ nm structure in the immediate vicinity of the mode crossing region. At $\theta=18^\circ$, around 12.5 GHz only 1LSM^P is evident in the BLS spectrum. The intensity of this mode is largely derived from the relatively large amplitude (U_3) of 1LSM^P that contributes to the ripple mediated scattering. The absence of the second mode, the hybridized-surface Lamb wave (H-SLW), at $\theta=18^\circ$ is due to its weaker U_3 component. As θ increases from 18° to 22° , stronger SLW- 1LSM^P hybridization results in enhancement of the U_3 amplitude of H-SLW, leading to the appearance of both coupled modes as a doublet in the BLS spectrum [Fig. 2(b)]. Hence as θ is gradually tuned within a narrow window $18^\circ \leq \theta \leq 22^\circ$ the relative strength of the doublet switches intensity reflecting the changing mode hybridization. Beyond $\theta > 24^\circ$, the hybridization is rapidly weakened and once again only 1LSM^P is observed in the light scattering spec-

trum. These changes in peak intensities are consistent with the calculated mode amplitudes U_1 and U_3 of H-SLW determined at $\theta=10^\circ$ and $\theta=20^\circ$ and illustrated in Fig. 2(c) in comparison to the corresponding amplitudes of 1LSM^p. Due to their smaller frequency separation, the corresponding doublet in the thicker membranes ($d_p=75$ and 110 nm) was barely resolved in the BLS spectra.

Flexural- or dilatational-type vibrations associated with the soft PMMA layer are not evident both in our experiments and calculations. Their nonappearance is due to the lower frequencies and large elastic mismatch between PMMA and Si₃N₄ layer. The resulting displacement profile within the PMMA layer has an approximate node at the interface leading to the absence of such flexural and dilatational type waves associated with the PMMA layer.

In conclusion, we have investigated the acoustic phonon properties of free standing double layer membranes composed of layers with distinctly different elastic properties. Detailed understanding of the acoustic modes in such free-standing structures and their BLS spectra provide for a non-destructive diagnostic method for evaluating the mechanical

properties of mesoscopic double layer systems. The spatial confinement of acoustic vibrations result in longitudinal and transverse standing wave resonances that are primarily confined within the soft PMMA layer at frequencies well below the fundamental resonance associated with the hard Si₃N₄ membrane. At higher frequencies the resonances permeate throughout the structure. At finite θ , modes whose amplitudes of vibration within the Si₃N₄ are consistent with flexural and dilatational modes for a single layer are observed to hybridize with the harmonics arising from the softer PMMA layer along certain propagation directions. The absence of corresponding low order surface Lamb modes associated with the PMMA layer illustrates that surface-related vibrations of an elastically soft freestanding membrane can be dramatically modified when tailored as a component within a double layer membrane.

Work at The Ohio State University was supported by the NSF under Grant No. DRM 0205521 and at the Naval Research Laboratory by the Office of Naval Research.

-
- ¹A. Erbe, H. Krommer, A. Kraus, R. H. Glick, G. Corso, and K. Richter, *Appl. Phys. Lett.* **77**, 3102 (2000).
- ²R. G. Beck, M. A. Eriksson, M. A. Topinka, R. M. Westervelt, K. D. Maranowski, and A. C. Gossard, *Appl. Phys. Lett.* **73**, 1149 (1998).
- ³J. G. E. Harris, D. D. Awschalom, F. Matsukara, H. Ohno, K. D. Maranowski, and A. C. Gossard, *Appl. Phys. Lett.* **74**, 1140 (1999).
- ⁴Y. T. Yang, K. Ekinici, X. M. H. Huang, L. M. Schiavone, M. L. Rokes, C. A. Zorman, and M. Mehregany, *Appl. Phys. Lett.* **78**, 162 (2001).
- ⁵T. P. Russel, *Science* **297**, 964 (2002); R. A. Matheson, *ibid.* **297**, 976 (2002).
- ⁶A. N. Cleland, M. Pophristic, and I. Ferguson, *Appl. Phys. Lett.* **79**, 2070 (2001).
- ⁷K. Schwab, E. A. Henricksson, J. M. Worlock, and M. Roukes, *Nature (London)* **404**, 974 (2000).
- ⁸L. P. Kouwenhoven and L. C. Venema, *Nature (London)* **404**, 944 (2000).
- ⁹B. A. Glavin, V. I. Pipa, V. V. Mitin, and M. A. Stroschio, *Phys. Rev. B* **65**, 205315 (2002).
- ¹⁰N. Bannov, V. Aristov, V. Mitin, and M. A. Stroschio, *Phys. Rev. B* **51**, 9930 (1995).
- ¹¹X. Zhang, R. Sooryakumar, and K. Bussman, *Phys. Rev. B* **68**, 115430 (2003).
- ¹²X. Zhang, J. D. Comins, A. G. Every, P. R. Stoddart, W. Pang, and T. E. Perry, *Phys. Rev. B* **58**, 13 677 (1998).
- ¹³G. Benedek, J. Ellis, A. Reichmuth, P. Ruggerone, H. Schief, and J. P. Toennies, *Phys. Rev. Lett.* **69**, 2951 (1992); D. Fuhrmann, E. Hulpke, and W. Steinhögl, *Phys. Rev. B* **57**, 4798 (1998); X. Zhang, R. Sooryakumar, A. G. Every, and M. H. Manghani, *ibid.* **64**, 081402 (2001).
- ¹⁴J. R. Dutcher, S. Lee, B. Hillebrands, G. J. McLaughlin, B. G. Nickel, and G. I. Stegeman, *Phys. Rev. Lett.* **68**, 2464 (1992).